Enhanced Thermochromic Properties of Vanadium Dioxide (VO$_2$)/Glass Heterostructure by Inserting a Zr-Based Thin Film Metallic Glasses (Cu$_{50}$Zr$_{50}$) Buffer Layer

Chaoyang Kang [1], Cong Zhang [1] , Yingxue Yao [2], Yuanjun Yang [2,*] , Haitao Zong [1], Liwei Zhang [1] and Ming Li [1]

[1] School of Physics and Electronic Information, Henan Polytechnic University, Jiaozuo 454000, China; kangcy@hpu.edu.cn (C.K.); czhang_94@163.com (C.Z.); haitaozong@163.com (H.Z.); lwzhang@hpu.edu.cn (L.Z.); mingli4587@aliyun.com (M.L.)
[2] School of Electronic Science and Applied Physics, Lab of Quantum Materials and Interfaces, Hefei University of Technology, Hefei 230009, China; yaoyingxue@mail.hfut.edu.cn
* Correspondence: yangyuanjun@hfut.edu.cn; Tel.: +86-551-62902024

check for updates

Featured Application: Smart windows and other transferable infrared devices.

Abstract: Vanadium dioxide (VO$_2$) with reversible metal–insulator transition (MIT) is one of the most promising energy-efficient materials. Especially for VO$_2$-based smart windows, the visible transmittance and solar modulation ability are the most critical parameters. However, VO$_2$ thin films that are directly deposited onto glass substrates are of poor crystallinity and MIT performance, limiting the practical applications of VO$_2$/glass heterostructures. In this paper, a buffer layer of Cu$_{50}$Zr$_{50}$ was introduced to build a novel Zr-based thin film metallic glass (VO$_2$/Cu$_{50}$Zr$_{50}$/glass) with multilayer structures for thermochromic applications. It is observed that the insertion of a Cu$_{50}$Zr$_{50}$ buffer layer with appropriate thickness results in a clear enhancement of crystalline quality and MIT performance in the VO$_2$/Cu$_{50}$Zr$_{50}$/glass thin films, compared with the single-layer VO$_2$/glass thin films. Moreover, the VO$_2$/Cu$_{50}$Zr$_{50}$/glass bi-layer films exhibit better optical performance with enhanced solar modulation ability (ΔT_{sol} = 14.3%) and a high visible transmittance (T_{vis} = 52.3%), which represents a good balance between ΔT_{sol} and T_{vis} for smart window applications.

Keywords: vanadium dioxide thin film; Cu$_{50}$Zr$_{50}$ buffer layers; metal–insulator transition; thermochromic property; smart window

1. Introduction

In response to a large energy-consuming and environmentally deteriorating condition, developing energy-saving materials and sustainable energy has aroused wide attention. Vanadium dioxide (VO$_2$) thin film is a first-order phase-changed material with superfast reaction speed that is near the critical temperature, 340 K [1,2]. This phase transformation is called a metal–insulator transition (MIT), and involves significant changes in electrical and optical characteristics. Its phase switching behavior makes VO$_2$ a hopeful candidate for a variety of applications, such as smart windows [3], sensor devices [4], ultrafast switches [5], Mott field effect transistors [4,6], etc.

Various techniques have been developed to form VO$_2$ thin films, for instance, molecular beam epitaxy [7], pulsed laser deposition [8], magnetron sputtering [9], and chemical vapor deposition [10]. Over the past decades, high-quality VO$_2$ thin films with the single crystalline characteristics have

been seeking because of the impact on MIT features. It is known that the characteristics of the chosen substrates play a major role in the thermochromic properties of VO_2 thin films [11,12]. A lot of single crystals have been employed to act as the growth substrates, such as titanium dioxide (TiO_2), silica (SiO_2), sapphire (Al_2O_3), and magnesium fluoride (MgF_2). The employ of single crystals results in a high expense for the device preparations and therefore immensely limits practical manufacture based on VO_2 thin films. As an alternative approach, common glass substrates with very low cost and good optical transmittance are potentially promising for the production of smart windows and other transferable infrared devices. However, VO_2 thin films that are directly grown onto conventional glass substrates are generally of poor crystallinity. Hence, single-layer VO_2/glass thin films have worse MIT and photoelectric properties [13,14]. In particular, the luminous transmittance and solar modulation ability are often especially bad in single-layer VO_2/glass structures, which limits the practical manufacture of VO_2-based smart windows. Thus, it is the need of the immediate to find a way to optimize the crystallinity and photoelectric properties in VO_2/glass heterostructures.

One way to do this is to design and fabricate a multilayered structure. Multilayered VO_2 thin films have been completed on different substrates by use of "buffer layers" of materials, such as TiO_2, SnO_2, ZnO [15–17], conductive oxides (Aluminum-doped Zinc Oxied (AZO), Fluorine Tin Oxide (FTO), Indium Tin Oxide (ITO), etc.) [18–20], metals (Ag, Cu, etc.), thin films [21], etc. Recently, thin film metallic glasses (TFMGs) were introduced and showed better surface roughness [22] and good optical properties [23,24]. In particular, Zr-based TFMG have received much scientific research attention for potential applications, since their good mechanical, tribological and fatigue properties, and their corrosion resistance and excellent adhesion [25–28]. Recently, Zong found that the Zr-based thin film metallic glasses ($Cu_{50}Zr_{50}$) have excellent near-infrared transmission (larger than 80%) [28]. $Cu_{50}Zr_{50}$, which can be prepared at room temperature, is a good candidate for template layers. The excellent near-infrared transmission and the appearance of the surface plasmon polaritons (SPPs) is anticipated to be favorable for the optical property of VO_2 thin films.

Motivated by the above demands for the thermochromic application of VO_2/glass thin films, in the present study we constructed a Zr-based thin film metallic glass (VO_2/$Cu_{50}Zr_{50}$/glass) with a multilayer structure, consisting of $Cu_{50}Zr_{50}$ TFMG as a buffer layer on amorphous glass substrates. The thickness dependence of the microstructure and optoelectronic properties of the VO_2/$Cu_{50}Zr_{50}$/glass multilayers was investigated. The achievements may be more comprehensive to understand the role of $Cu_{50}Zr_{50}$ buffer layers in the formation of high-crystalline VO_2 thin films on glass substrates, and thus pave a way towards heightening the photoelectrical properties of VO_2 thin film-based devices.

2. Experimental

2.1. Method for Film Deposition

VO_2/glass monolayer and VO_2/$Cu_{50}Zr_{50}$/glass bilayer structures (different $Cu_{50}Zr_{50}$ buffer layer thicknesses) were prepared by pulsed laser deposition (wavelength 248 nm). The targets are V (99.95% purity, 25 mm diameter, 3 mm thick) and $Cu_{50}Zr_{50}$ alloy (99.99% purity, 40 mm diameter, 5 mm thick). Cleaned the amorphous glass substrates (BF33) with an ethanol/acetone solution, rinsed with distilled water, and finally blown with pure nitrogen. Prior to deposition, the base pressure was controlled at 1.0×10^{-4} Pa and the target-substrate distance was 6 cm. During the deposition, the laser operated at repetition rate of 5 Hz and output pulse energy of 200 mJ for entire deposition, the target and substrate were rotated at a rate of 18 rpm. The deposition conditions for the VO_2 film and buffer layer were 500 °C with P_{O2} = 0.9 Pa for VO_2 film, room temperature without oxygen inlet for $Cu_{50}Zr_{50}$. The oxygen flow rate was 25 sccm for VO_2. The film thickness was controlled by deposition time and corrected by step profiler (DektakXT, Bruker, Karlsruhe, Germany). The $Cu_{50}Zr_{50}$ buffer layers had thicknesses of 40 nm, 80 nm, and 160 nm in the three multilayer VO_2/$Cu_{50}Zr_{50}$/glass thin films. For comparison, the single-layer VO_2 thin films were grown directly on an amorphous glass substrate

under the same conditions as the $VO_2/Cu_{50}Zr_{50}/glass$ thin films. The thickness of all the VO_2 thin films was 60 nm. The four thin films were marked as $VO_2(60\ nm)/glass$, $VO_2(60\ nm)/Cu_{50}Zr_{50}(40\ nm)/glass$, $VO_2(60\ nm)/Cu_{50}Zr_{50}(80\ nm)/glass$, and $VO_2(60\ nm)/Cu_{50}Zr_{50}(160\ nm)/glass$.

2.2. Film Characterization

The crystallographic properties of the sample was characterized by X-ray diffraction (XRD) using a instrument modeled LabXRD-6000 (Shimadzu, Kyushu, Japan) (λ = 0.15406 nm). Using atomic force microscopy (AFM), the surface morphology of the samples was studied with a profilometer (Dektak 150, Bruker, Karlsruhe, Germany)). Images were additionally acquired by scanning electron microscopy (SEM) (Zeiss Supa 50VP, Jena Germany). The temperature-driven MIT properties were measured during the heating and cooling process within the temperature range 30–120 °C by the Hall Effect Measurement System (HMS-5300, Ecopia, Pyeongchang, South Korea). A double beam spectrophotometer (UV-3600, Shimadzu, Kyushu, Japan) with a spectral range of 200–2650 nm was used to record the transmittance spectra of the films. The temperature was controlled in situ by a heater.

3. Results and Discussion

3.1. Microstructural Properties

Figure 1 shows the XRD diffraction patterns of the $VO_2/glass$ film and $VO_2/Cu_{50}Zr_{50}/glass$ films. The generalized diffraction with the 2θ ranging from 15° to 30° indicates the glass properties of the substrates. For the thin films, the peaks that were located at 27.80° are attributed to the VO_2 (011) peak (JCPDS No. 43-1051), which is the feature diffraction peak for M1-phase VO_2 thin films [29]. All of the VO_2 thin films are strongly oriented along the [011] direction, whether or not buffer layers were inserted on the glass substrate. The diffraction peak located at 31.47° belongs to the ZrO_2 (111) peak (JCPDS No. 65-1024), implying the monoclinic symmetry characteristics of the ZrO_2. The peak located at 42.42° is assigned to the Cu_2O (200) peak (JCPDS No. 77-0199). The appearance of ZrO_2 and Cu_2O may be due to the incorporation of Zr and Cu ions with oxygen during the VO_2 thin film growth. In addition, as the thickness of the buffer layer increases, the intensity of VO_2 (011) peaks (in units of counts per second (cps)) initially increases and then decreases, indicating that the crystal quality of VO_2 thin films initially improves and then worsens. The characteristic peaks of the VO_2 phase disappear in the 160 nm-thick $VO_2/Cu_{50}Zr_{50}/glass$ thin films, which clearly indicates that thicker buffer layers make VO_2 amorphous.
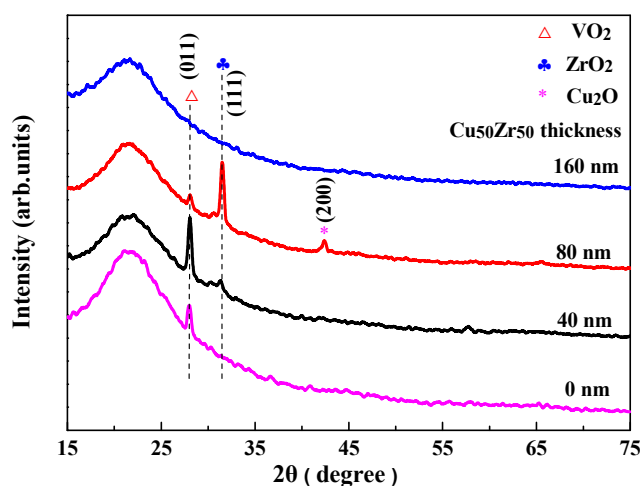

Figure 1. X-ray diffraction (XRD) patterns of vanadium dioxide (VO_2) films deposited on $Cu_{50}Zr_{50}$ buffer layers with different thicknesses.

Figure 2 shows the AFM micrographs of the surfaces of the VO_2/glass film and VO_2/$Cu_{50}Zr_{50}$/glass films. The surfaces of the VO_2/$Cu_{50}Zr_{50}$/glass films are smoother and more uniform than the VO_2/glass film. The measured roughnesses of the VO_2/$Cu_{50}Zr_{50}$/glass films without a buffer layer, and with buffer layers with thicknesses of 40 nm, 80 nm, and 160 nm, are 2.86 nm, 1.32 nm, 1.51 nm, and 2.12 nm, respectively, indicating that the surface morphology of VO_2 films that are grown on glass substrates can be optimized effectively by embedding a $Cu_{50}Zr_{50}$ buffer layer. What calls for special attention is a suitable thickness needs that the $Cu_{50}Zr_{50}$ buffer layer need to select, since excess thickness of $Cu_{50}Zr_{50}$ layers will generate rougher films.

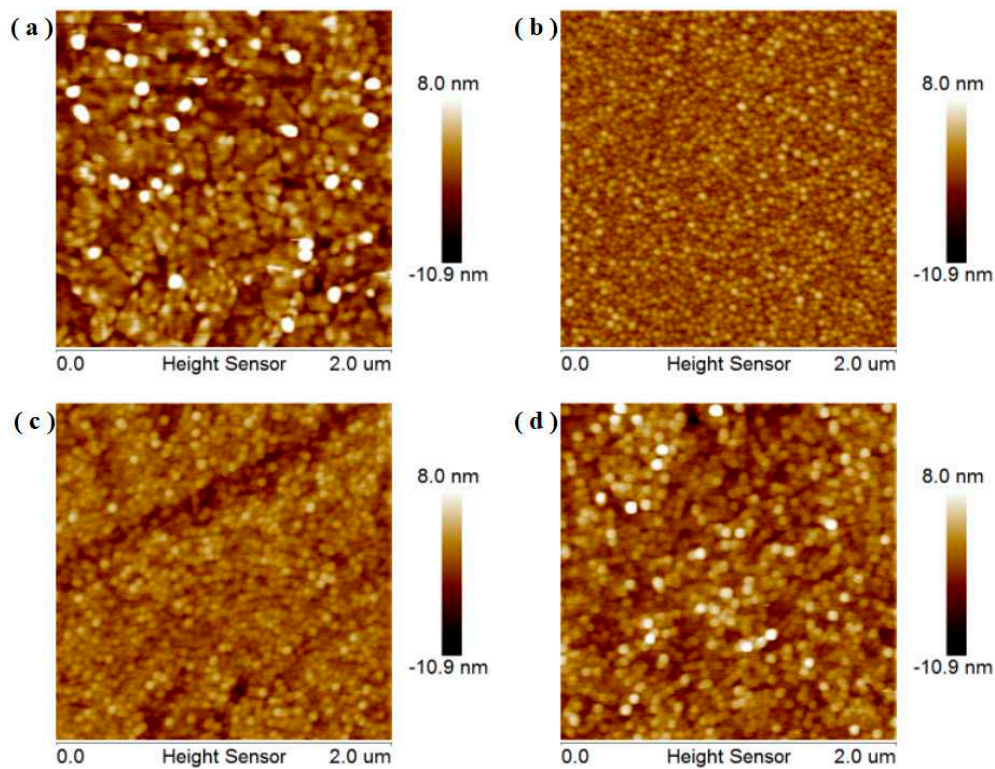**Figure 2.** Atomic force microscopy (AFM) images of the Zr-based thin film metallic glass (VO_2/$Cu_{50}Zr_{50}$/glass) thin films with different $Cu_{50}Zr_{50}$ thicknesses. (**a**) No thin film; (**b**) 40 nm thickness; (**c**) 80 nm thickness; and (**d**) 160 nm thickness.

To further show the effects of the buffer layer thickness on the microstructures, the SEM images of the surface morphology of the VO_2/$Cu_{50}Zr_{50}$/glass thin films with different buffer layer thicknesses are shown in Figure 3. The surfaces of all the films are found to be continuous and dense. The bright white segments that are visible on the surface of films are identified as amorphous metal V particles, according to the elemental analysis illustrated in the small red circles of Figure 3c,d by Energy-dispersive X-ray spectroscopy (EDS). After embedding an alloy buffer layer, the number of the amorphous metal V particles increases clearly, resulting in poor crystallinity of the VO_2 thin films on the thick buffer layer.

By combining the above analysis, the following can be conjectured. When the buffer layer thickness is relatively thin (~40 nm), the incorporation of Zr atoms with O atoms during deposition forms monoclinic ZrO_2. The ZrO_2 interfacial layer serves as a template to improve the crystallinity of the upper VO_2 thin films. This result is highly consistent with the case of the VO_2/Y-doped ZrO_2/Si thin films [30], where the Y-doped ZrO_2 served as the buffer layer. As the buffer layer thickness increases to 80 nm, the high roughness and impure phase of Cu_2O deteriorates the crystal quality of the VO_2 thin films. When the buffer layer thickness increases to 160 nm, much more oxygen is

consumed and too many amorphous metal V particles are present on the film surface, which reduces the crystalline quality of the VO_2(M) thin film.
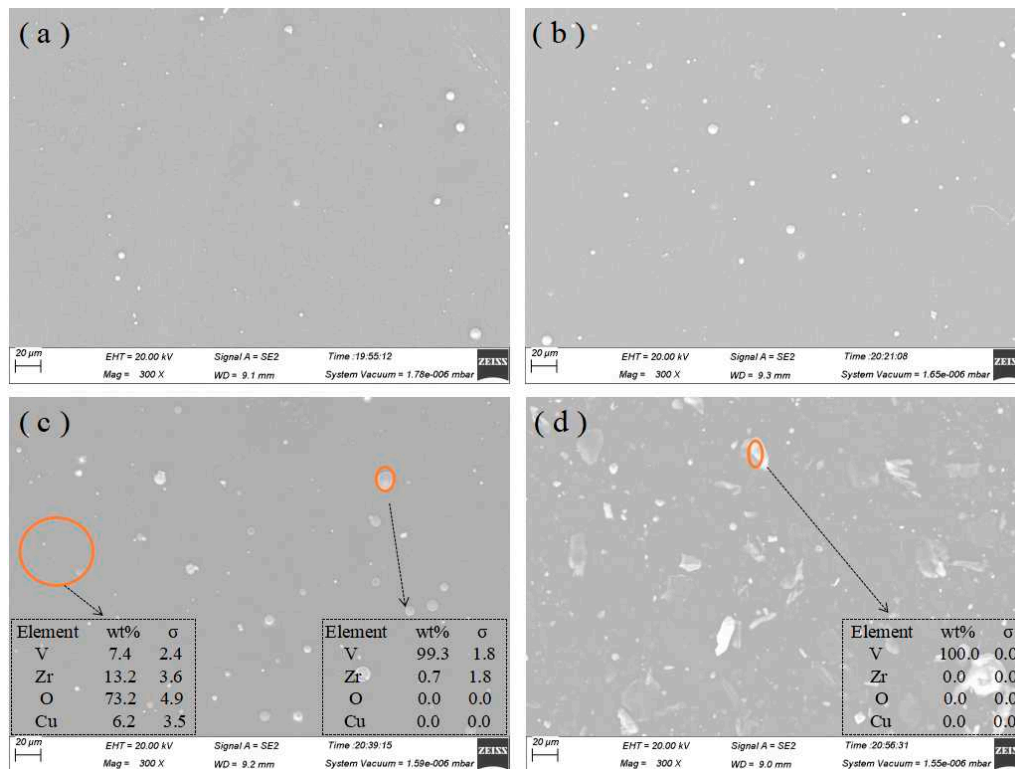

Figure 3. Scanning electron microscopy (SEM) images and Energy-dispersive X-ray spectroscopy (EDS) element distribution table (insets) of VO_2 films deposited on $Cu_{50}Zr_{50}$ buffer layers with different thicknesses. (**a**) No buffer layer (**b**) 40 nm thickness (**c**) 80 nm thickness (**d**) 160 nm thickness.

3.2. Electrical Properties

Figure 4 shows the square resistance variation with temperature in the heating and cooling cycles of the VO_2 thin films with various thicknesses of $Cu_{50}Zr_{50}$ inserting buffer layers. In Figure 4a, the VO_2/glass thin films show a resistance–temperature curve with a wide transformation hysteresis. In the cases of the 40- and 80-nm-thick buffer layers, the VO_2 thin films both exhibit sharper decreases in sheet resistance with increasing temperature, as illustrated in Figure 4b,c, strongly implying the occurrence of an MIT. However, no MIT occurs when the buffer layer thickness attains to 160 nm. This result can be attributed to poor crystallization in the VO_2/$Cu_{50}Zr_{50}$/glass thin films, which is good corresponding to the XRD analysis.

To better comparing, the observed electrical properties of VO_2 films with various buffer layer thicknesses are summarized in Table 1. The transition temperature (T_c) is defined as the center of the derivative curve of the heating curve in the insets of Figure 3. Here, we defined the amplitude of MIT (ΔR) as the relative resistance change ratio between room temperature and a temperature of 100 °C. The hysteresis width (ΔH) is the difference between the T_c values that were measured during the heating and cooling cycles. From Table 1, the single-layer VO_2 thin films have higher T_c than the buffered VO_2 thin films. After introducing the buffer layer (40 nm and 80 nm in thickness), the T_c values of VO_2 thin films are similar to that of the bulk VO_2 single crystal (68 °C), which is generally due to the release of stress [31]. The ΔR values of the VO_2/glass thin films are slightly larger than those of the 40- and 80-nm-thick VO_2/$Cu_{50}Zr_{50}$/glass thin films. This could be due to the larger crystal size in the non-buffered VO_2 thin films [32]. The samples with smaller or larger ΔH values can be applied in different fields and the ΔH value is closely connected with the quality of crystallization and crystallite

dimension in the VO$_2$ thin films [33–35]. From Table 1, it can be seen that the ΔH values of the buffered VO$_2$ thin films are much smaller than the non-buffered one. The buffer layer serves as a good template for VO$_2$ thin film growth and it thus results in a better crystallinity in the 40- and 80-nm-thick VO$_2$/Cu$_{50}$Zr$_{50}$/glass thin films. These conclusions point out that the electrical characteristic of VO$_2$ films can be significantly enhanced by inserting Cu$_{50}$Zr$_{50}$ buffer layer of appropriate thickness.
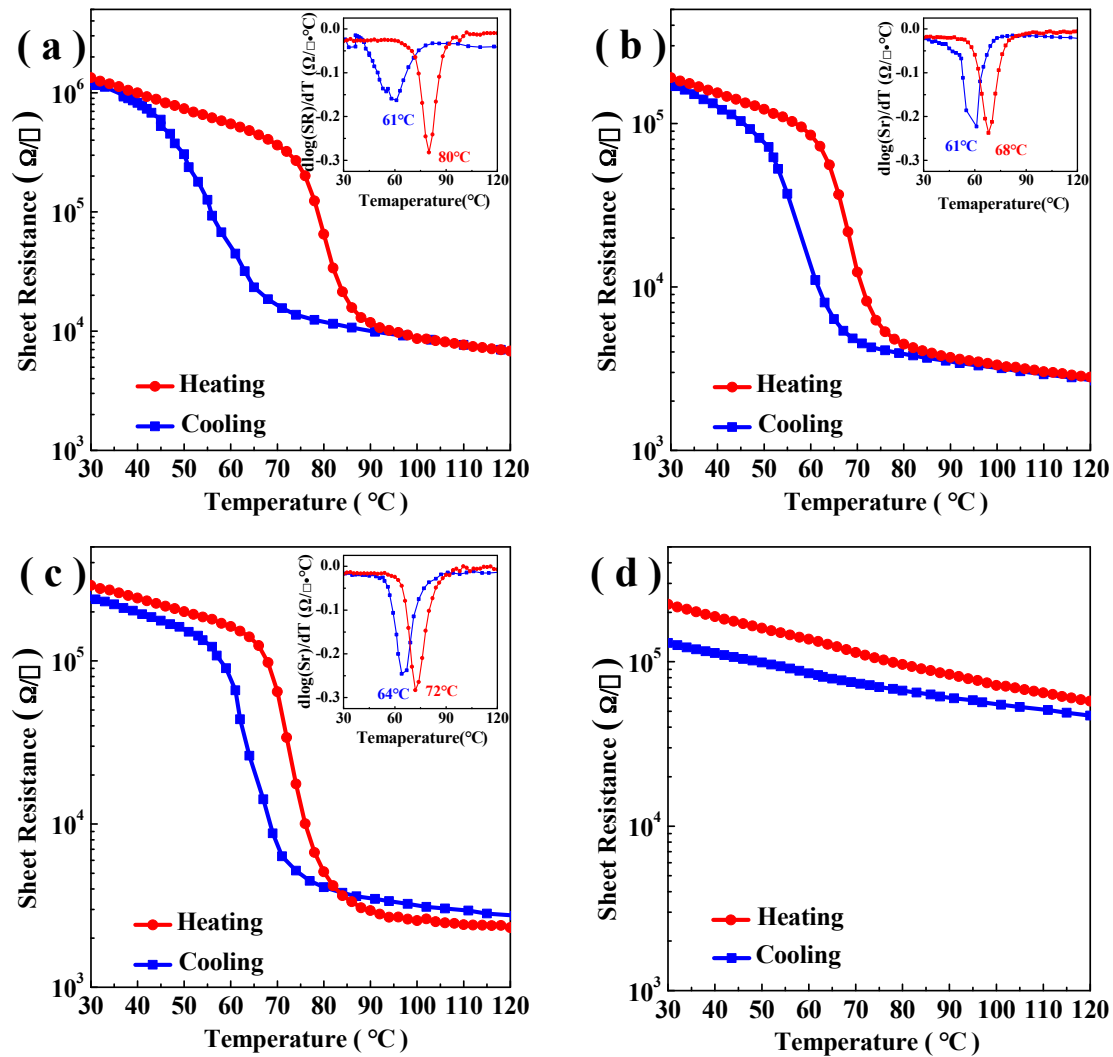

Figure 4. Temperature-dependent sheet resistance of the VO$_2$/Cu$_{50}$Zr$_{50}$/glass thin films with different buffer layer thicknesses. (**a**) No film; (**b**) 40 nm thickness; (**c**) 80 nm thickness; and, (**d**) 160 nm thickness. The insets d(lgR)/dT ~T are also shown to determine metal–insulator transition (MIT) temperatures.

Table 1. Thermochromic transition characteristics of the multilayer VO$_2$/Cu$_{50}$Zr$_{50}$/glass thin films.

Thickness of Cu$_{50}$Zr$_{50}$ Buffer Layer (nm)	0 nm	40 nm	80 nm
Transition temperature, Tc	80 °C	68 °C	72 °C
Resistance change, ΔR	2×10^2	0.7×10^2	1.2×10^2
Hysteresis width, ΔH	19 °C	7 °C	8 °C

3.3. Optical Properties

The optical parameters of VO$_2$/glass and VO$_2$/Cu$_{50}$Zr$_{50}$/glass thin films is measured with in situ varying temperature. Figure 5 depicts the thermochromic transmittance curves of VO$_2$/glass

and VO$_2$/Cu$_{50}$Zr$_{50}$/glass films in response to preset temperatures (from room temperature to 100 °C). Objectively speaking, the transmittance of all the samples in the visible region is almost constant. However, the transmittance of VO$_2$(60 nm)/glass, VO$_2$(60 nm)/Cu$_{50}$Zr$_{50}$(40 nm)/glass, and VO$_2$(60 nm)/Cu$_{50}$Zr$_{50}$(80 nm)/glass decreases clearly with the temperature increases in the infrared region, as shown in Figure 5a–c, while in the VO$_2$(60 nm)/Cu$_{50}$Zr$_{50}$(160 nm)/glass thin films the transmittance changes relatively little (Figure 5d).
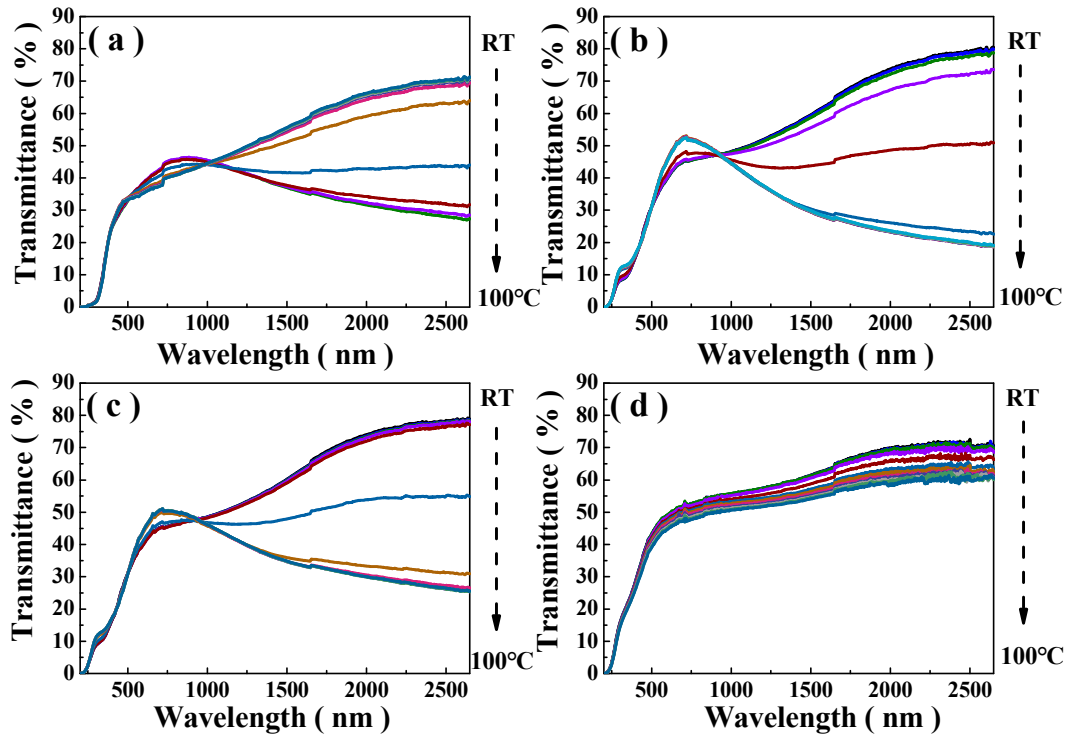

Figure 5. Optical transmittance curves of the VO$_2$/Cu$_{50}$Zr$_{50}$/glass thin films in the range of 200–2650 nm by varying temperature, for various thicknesses of Cu$_{50}$Zr$_{50}$ buffer layer. (**a**) No layer; (**b**) 40 nm thickness; (**c**) 80 nm thickness; and (**d**) 160 nm thickness.

The optical modulation properties of the VO$_2$ thin film are investigated to evaluate its potential in smart windows. In order to realize the applications of VO$_2$ in smart windows, technological challenges need to be addressed, including improving the maximum visible transmittance (T_{vis}), maintaining high solar modulating efficiency (ΔT_{sol}), and undergoing more than 10,000 cycles without any degradation [36]. The T_{vis}, ΔT_{sol}, and near-infrared (NIR) switching efficiency (ΔT_{2500nm}) of all the samples were obtained by the calculation of the transmittance spectra and are displayed in Figure 6. The solar transmittance (T_{sol}, 300–2500 nm) and the ΔT_{sol} values are derived from the following formulas:

$$T_{sol} = \frac{\int \varphi sol(\lambda)T(\lambda)\mathrm{d}\lambda}{\int \varphi sol(\lambda)\mathrm{d}\lambda} \tag{1}$$

$$\Delta T_{sol} = T_{sol(30\,°C)} - T_{sol(100\,°C)} \tag{2}$$

where $T(\lambda)$ is defined as the transmittance at wavelength λ and φ_{sol} is the solar irradiance spectrum for air mass 1.5 (corresponding to the sun standing 37° above the horizon) [37]. As shown in Figure 6, the T_{vis}, ΔT_{sol}, and ΔT_{2500nm} values of the monolayer VO$_2$ film are 44.6%, 7.2% and 42.7%, respectively. Therefore, the good thermochromic properties with enhanced luminous transmittance is obtained by introducing Cu$_{50}$Zr$_{50}$ as buffer layer, possibly because Cu$_{50}$Zr$_{50}$ can act as an anti-reflection layer (AR) for VO$_2$ films. When compared with the VO$_2$(60 nm)/glass, the samples of VO$_2$(60 nm)/Cu$_{50}$Zr$_{50}$(40 nm)/glass and VO$_2$(60 nm)/Cu$_{50}$Zr$_{50}$(80 nm)/glass have higher ΔT_{sol} and

ΔT_{2500nm} values. According to [28], $Cu_{50}Zr_{50}$ possesses a metallic property in the infrared region. For the sandwich structure $VO_2/Cu_{50}Zr_{50}/glass$, p-polarized SPPs are supported on the metallic film interfaces in the corresponding range. The appearance of the SPPs probably effectively modulates the optical properties. This mechanism will be further studied in the future [38,39]. When increasing the $Cu_{50}Zr_{50}$ buffer layer thickness to 160 nm, the ΔT_{sol} and ΔT_{2500nm} values clearly decreased. The main reason for this is the effect of crystallization quality, which corresponds to the above XRD data analysis. Favorable thermochromic properties are achieved in the sample of $VO_2(60\ nm)/Cu_{50}Zr_{50}(40\ nm)/glass$. The sample of $VO_2(60\ nm)/Cu_{50}Zr_{50}(40\ nm)/glass$ shows better optical thermochromic performance, and the ΔT_{sol} value is as high as ~14.3% with the T_{vis} value up to 52.3% and the ΔT_{2500nm} value up to 60.2%, which represents a good balance between ΔT_{sol} and T_{vis} for smart window applications. These results can be compared with previous experimental results, such as those for periodic and aperiodic porous $VO_2(M1)$ films that were prepared through complex chemical and physical processes in multiple layers of $TiO_2(or\ SiO_2)/VO_2/substrate$ films [40–42] and VO_2-based composite thin films [43,44]. All in all, optimizing optical properties of VO_2 films had indeed been enhanced by the introduction of $Cu_{50}Zr_{50}$ buffer layer.
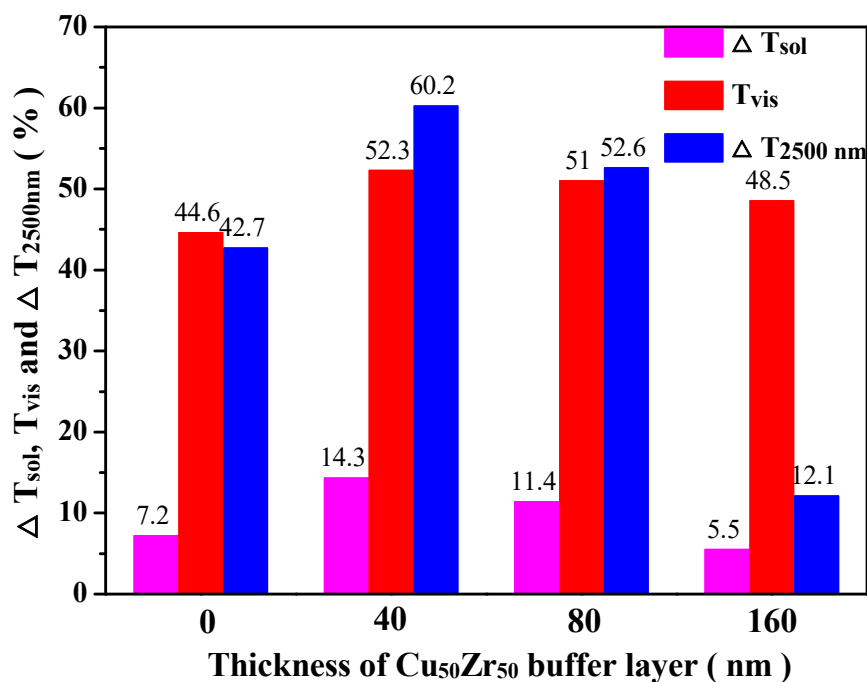

Figure 6. Summarized optical properties of the $VO_2/Cu_{50}Zr_{50}/glass$ thin films with different buffer layer thicknesses.

4. Conclusions

To conclude, VO_2 thin films with monoclinic crystal phase are here successfully grown on glass substrates by PLD (Plused Laser Deposition) techniques. $Cu_{50}Zr_{50}$ buffer layers of various thicknesses were introduced to modulate the MIT and optical properties. It is observed that a pronounced smaller ΔH across the MIT is achieved in the optimized $VO_2 (60\ nm)/Cu_{50}Zr_{50}(40\ nm)/glass$ film. The ΔT_{sol} value is as high as ~14.3%, with the T_{vis} value up to 52.3%. A ΔT_{2500nm} value of up to 60.2% is achieved in the $VO_2 (60\ nm)/Cu_{50}Zr_{50}(40\ nm)/glass$ film. The present study suggests that the introduction of a $Cu_{50}Zr_{50}$ buffer layer of appropriate thickness on a glass substrate is beneficial to the improvement of crystalline quality and thermochronic properties of VO_2 thin films, which makes VO_2 a candidate material for use in photoelectronic devices and smart windows.

References

1. Morin, F.J. Oxides which show a metal-to-insulator transition at the neel temperature. *Phys. Rev. Lett.* **1959**, *3*, 34–36. [CrossRef]

2. Chen, W.; Zhang, Y.Z.; Zhang, C.J.; Zhu, L.G.; Wang, S.M.; Wang, B.X. Thermomechanical analysis and optimisation for beam blank continuous casting. *Ironmak. Steelmak.* **2013**, *35*, 129–136. [CrossRef]

3. Wang, S.; Liu, M.; Kong, L.; Long, Y.; Jiang, X.; Yu, A. Recent progress in VO_2, smart coatings: strategies to improve the thermochromic properties. *Prog. Mater. Sci.* **2016**, *81*, 1–54. [CrossRef]

4. Kim, H.T.; Chae, B.G.; Youn, D.H.; Maeng, S.L.; Kim, G.; Kang, K.Y.; Lim, Y.S. Mechanism and observation of mott transition in VO_2-based two-and three-terminal devices. *New J. Phys.* **2004**, *6*, 52. [CrossRef]

5. Cavalleri, A.; Tóth, C.; Siders, C.W.; Squier, J.A.; Ráksi, F.; Forget, P.; Kieffer, J.C. Femtosecond structural dynamics in VO_2 during an ultrafast solid-solid phase transition. *Phys. Rev. Lett.* **2001**, *87*, 237401. [CrossRef] [PubMed]

6. Zhou, C.; Newns, D.M.; Misewich, J.A.; Pattnaik, P.C. A field effect transistor based on the Mott transition in a molecular layer. *Appl. Phys. Lett.* **1997**, *70*, 598–600. [CrossRef]

7. Bian, J.M.; Wang, M.H.; Sun, H.J.; Liu, H.Z.; Li, X.X.; Luo, Y.M.; Zhang, Y.Z. Thickness-Modulated Metal–Insulator Transition of VO_2 Film Grown On Sapphire Substrate by MBE. *J. Mater. Sci.* **2016**, *51*, 6149–6155. [CrossRef]

8. Jian, J.; Wang, X.J.; Li, L.G.; Fan, M.; Zhang, W.; Huang, J.J.; Qi, Z.M.; Wang, H.Y. Continuous Tuning of Phase Transition Temperature in VO_2 Thin Films On c-Cut Sapphire Substrates Via Strain Variation. *ACS Appl. Mater. Inter.* **2017**, *9*, 5319–5327. [CrossRef] [PubMed]

9. Yang, Y.J.; Wang, L.X.; Huang, H.L.; Kang, C.Y.; Zong, H.T.; Zou, C.W.; Lu, Y.L.; Li, X.G.; Hong, B.; Gao, C. Controlling Metal-Insulator Transition in (010)-VO_2/(0001)-Al_2O_3 Epitaxial Thin Film through Surface Morphological Engineering. *Ceram. Int.* **2018**, *44*, 3348–3355. [CrossRef]

10. Zhou, H.J.; Li, J.H.; Xin, Y.C.; Cao, X.; Bao, S.H.; Jin, P. Electron Transfer Induced Thermochromism in a VO_2-graphene-Ge Heterostructure. *J. Mater. Chem. C* **2015**, *3*, 589–597. [CrossRef]

11. Babkin, E.V.; Charyev, A.A.; Dolgarev, A.P.; Urinov, H.O. Metal-insulator phase transition in VO_2: influence of film thickness and substrate. *Thin Solid Films* **1987**, *150*, 11–14. [CrossRef]

12. György, J.K.; Danilo, B.; Ilona, S.; Helfried, R.; René, H.; Heidemarie, S. Effect of the substrate on the insulator–metal transition of vanadium dioxide films. *J. Appl. Phys.* **2011**, *109*, 582.

13. Muraoka, Y.; Hiroi, Z. Metal–insulator transition of VO_2 thin films grown on TiO_2 (001) and (110) substrates. *Appl. Phys. Lett.* **2002**, *80*, 583–585. [CrossRef]

14. Nagashima, K.; Yanagida, T.; Tanaka, H.; Kawai, T. Interface effect on metal-insulator transition of strained vanadium dioxide ultrathin films. *J. Appl. Phys.* **2007**, *101*, 34. [CrossRef]

15. Zhang, D.; Yang, K.; Li, Y.; Liu, Y.; Zhu, M.; Zhong, A.; Cai, X.; Fan, P.; Lv, W. Employing TiO_2 buffer layer to improve VO_2 film phase transition performance and infrared solar energy modulation ability. *J. Alloys Compd.* **2016**, *684*, 719–725. [CrossRef]

16. Panagopoulou, M.; Gagaoudakis, E.; Aperathitis, E.; Michail, I.; Kiriakidis, G.; Tsoukalas, D.; Raptis, Y.S. The effect of buffer layer on the thermochromic properties of undoped radio frequency sputtered VO_2 thin films. *Thin Solid Films* **2015**, *594*, 310–315. [CrossRef]

17. Zhu, M.; Qi, H.; Wang, B.; Wang, H.; Guan, T.; Zhang, D. Thermochromism of vanadium dioxide films controlled by the thickness of ZnO buffer layer under low substrate temperature. *J. Alloys Compd.* **2018**, *740*, 844–851. [CrossRef]

18. Sato, K.; Hoshino, H.; Mian, M.S.; Okimura, K. Low-temperature growth of VO$_2$ films on transparent ZnO/glass and al-doped ZnO/glass and their optical transition properties. *Thin Solid Films* **2018**, *651*, 91–96. [CrossRef]

19. Zhang, Z.; Gao, Y.; Luo, H.; Kang, L.; Chen, Z.; Du, J.; Kanehira, M.; Zhang, Y.Z.; Wang, Z.L. Solution-based fabrication of vanadium dioxide on F:SnO$_2$ substrates with largely enhanced thermochromism and low-emissivity for energy-saving applications. *Energy Environ. Sci.* **2011**, *4*, 4290–4297. [CrossRef]

20. Beydaghyan, G.; Basque, V.; Ashrit, P.V. High contrast thermochromic switching in vanadium dioxide (VO$_2$) thin films deposited on indium tin oxide substrates. *Thin Solid Films* **2012**, *522*, 204–207. [CrossRef]

21. Voti, R.L.; Larciprete, M.C.; Leahu, G.; Sibilia, C.; Bertolotti, M. Optical response of multilayer thermochromic VO$_2$-based structures. *J. Nanophotonics* **2015**, *6*, 5752–5757.

22. Chu, C.W.; Jang, J.S.C.; Chen, G.J.; Chiu, S.M. Characteristic studies on the Zr-based metallic glass thin film fabricated by magnetron sputtering process. *Surf. Coat. Technol.* **2008**, *202*, 5564–5566. [CrossRef]

23. Liu, Y.; Hata, S.; Wada, K.; Shimokohbe, A. Thermal, mechanical and electrical properties of Pd-based thin-film metallic glass. *Jpn. J. Appl. Phys.* **2001**, *40*, 5382. [CrossRef]

24. Chu, J.P.; Liu, C.T.; Mahalingam, T.; Wang, S.F.; O'Keefe, M.J.; Johnson, B.; Kuo, C.H. Annealing-induced full amorphization in a multicomponent metallic film. *Phys. Rev. B* **2004**, *69*, 113410. [CrossRef]

25. Liu, F.X.; Yang, F.Q.; Gao, Y.F.; Jiang, W.H.; Guan, Y.F.; Rack, P.D.; Liaw, P.K. Micro-scratch study of a magnetron-sputtered Zr-based metallic-glass film. *Surf. Coat. Technol.* **2009**, *203*, 3480–3484. [CrossRef]

26. Lee, C.J.; Lin, H.K.; Sun, S.Y.; Huang, J.C. Characteristic difference between ITO/ZrCu and ITO/Ag bi-layer films as transparent electrodes deposited on pet substrate. *Appl. Surf. Sci.* **2010**, *257*, 239–243. [CrossRef]

27. Cheng, J.Y.; Kang, C.Y.; Zong, H.T.; Cao, G.H.; Li, M. Structural and photoelectrical properties of AZO thin films improved by Ag buffer layers. *Acta Phys. Sin.* **2017**, *66*, 027702.

28. Zong, H.; Geng, C.; Kang, C.; Cao, G.; Li, L.; Zhang, B.; Li, M. Excellent near-infrared transmission of Zr-based thin film metallic glasses. *Results Phys.* **2018**, *10*, 612–615. [CrossRef]

29. Yang, Z.; Ko, C.; Ramanathan, S. Metal-insulator transition characteristics of VO$_2$ thin films grown on Ge (100) single crystals. *J. Appl. Phys.* **2010**, *108*, 073708. [CrossRef]

30. Gupta, A.; Aggarwal, R.; Gupta, P.; Dutta, T.; Narayan, J.; Narayan, J. Semiconductor to metal transition characteristics of thin films grown epitaxially on Si (001). *Appl. Phys. Lett.* **2009**, *95*, 111915. [CrossRef]

31. Koo, H.; Yoon, S.; Kwon, O.J.; Ko, K.E.; Shin, D.; Bae, S.H.; Chang, S.H.; Park, C. Effect of lattice misfit on the transition temperature of VO$_2$ thin film. *J. Mater. Sci.* **2012**, *47*, 6397–6401. [CrossRef]

32. Wang, L.X.; Yang, Y.J.; Zhao, J.G.; Hong, B.; Hu, K.; Peng, J.L.; Zhang, H.B.; Wen, X.L.; Luo, Z.L.; Li, X.G.; et al. Growth temperature-dependent metal–insulator transition of vanadium dioxide epitaxial films on perovskite strontium titanate (111) single crystals. *J. Appl. Phys.* **2016**, *119*, 145301. [CrossRef]

33. Zhi, B.; Gao, G.Y.; Tan, X.L.; Chen, P.F.; Wang, L.F.; Jin, S.W.; Wu, W.B. Thickness-dependent metal-to-insulator transition in epitaxial VO$_2$ films. *Mater. Res. Express* **2014**, *1*, 046402. [CrossRef]

34. Appavoo, K.; Lei, D.Y.; Sonnefraud, Y.; Wang, B.; Pantelides, S.T.; Maier, S.A.; Haglund, R.F., Jr. Role of defects in the phase transition of VO$_2$ nanoparticles probed by plasmon resonance spectroscopy. *Nano Lett.* **2012**, *12*, 780–786. [CrossRef] [PubMed]

35. Jostmeier, T.; Zimmer, J.; Karl, H.; Krenner, H.J.; Betz, M. Optically imprinted reconfigurable photonic elements in a VO$_2$ nanocomposite. *Appl. Phys. Lett.* **2014**, *105*, 071107.

36. Zhou, M.; Bao, J.; Tao, M.; Zhu, R.; Lin, Y.; Zhang, X.; Xie, Y. Periodic porous thermochromic VO$_2$(M) films with enhanced visible transmittance. *Chem. Commun.* **2013**, *49*, 6021–6023. [CrossRef] [PubMed]

37. American Society for Testing and Materials (ASTM). *G173-03: Standard Tables for Reference Solar Spectral Irradiances: Direct Normal and Hemispherical on 37° Tilted Surface*; Annual Book of ASTM Standards; American Society for Testing and Materials: West Conshohocken, PA, USA, 2008; Vol. 14.04.

38. Jostmeier, T.; Mangold, M.; Zimmer, J.; Karl, H.; Krenner, H.J.; Ruppert, C.; Betz, M. Thermochromic modulation of surface plasmon polaritons in vanadium dioxide nanocomposites. *Opt. Express* **2016**, *24*, 17321–17331. [CrossRef] [PubMed]

39. Markov, P.; Appavoo, K.; Haglund, R.F., Jr.; Weiss, S.M. Hybrid Si-VO(2)-Au optical modulator based on near-field plasmonic coupling. *Opt. Express* **2015**, *23*, 6878–6887. [CrossRef] [PubMed]

40. Sun, Y.; Xiao, X.; Xu, G.; Dong, G.; Chai, G.; Zhang, H.; Liu, P.Y.; Zhu, H.M.; Zhan, Y.J. Anisotropic vanadium dioxide sculptured thin films with superior thermochromic properties. *Sci. Rep.* **2013**, *3*, 2756. [CrossRef] [PubMed]

41. Chen, Z.; Gao, Y.; Kang, L.; Cao, C.; Chen, S.; Luo, H. Fine crystalline VO$_2$ nanoparticles: Synthesis, abnormal phase transition temperatures and excellent optical properties of a derived VO$_2$ nanocomposite foil. *J. Mater. Chem. A* **2014**, *2*, 2718–2727. [CrossRef]

42. Zheng, J.; Bao, S.; Jin, P. TiO$_2$(R)/VO$_2$(M)/TiO$_2$(A) multilayer film as smart window: combination of energy-saving, antifogging and self-cleaning functions. *Nano Energy* **2015**, *11*, 136–145. [CrossRef]

43. Gao, Y.F.; Wang, S.B.; Dai, L.; Cao, C.X.; Luo, H.J.; Minoru, K. VO$_2$–Sb:SnO$_2$ composite thermochromic smart glass foil. *Energy Environ. Sci.* **2012**, *5*, 8234–8237. [CrossRef]

44. Li, M.; Wu, X.; Li, L.; Wang, Y.; Li, D.; Pan, J.; Li, S.J.; Sun, L.T.; Li, G.H. Defect-mediated phase transition temperature of VO$_2$(M) nanoparticles with excellent thermochromic performance and low threshold voltage. *J. Mater. Chem. A* **2014**, *2*, 4520–4523. [CrossRef]